

# Geometry and electronic structure of impurity-trapped excitons in $\text{Cs}_2\text{GeF}_6:\text{U}^{4+}$ crystals. The $5f^17s^1$ manifold

Belén Ordejón

*Departamento de Química, C-XIV, Universidad Autónoma de Madrid, 28049 Madrid, Spain*

Luis Seijo and Zoila Barandiarán<sup>a)</sup>

*Departamento de Química, C-XIV, Universidad Autónoma de Madrid, 28049 Madrid, Spain  
and Instituto Universitario de Ciencia de Materiales Nicolás Cabrera, Universidad Autónoma de Madrid, 28049 Madrid, Spain*

(Received 31 January 2007; accepted 10 April 2007; published online 21 May 2007)

Excitons trapped at impurity centers in highly ionic crystals were first described by McClure and Pédrini [Phys. Rev. B **32**, 8465 (1985)] as excited states consisting of a bound electron-hole pair with the hole localized on the impurity and the electron on nearby lattice sites, and a very short impurity-ligand bond length. In this work the authors present a detailed microscopic characterization of impurity-trapped excitons in  $\text{U}^{4+}$ -doped  $\text{Cs}_2\text{GeF}_6$ . Their electronic structure has been studied by means of relativistic *ab initio* model potential embedded cluster calculations on  $(\text{UF}_6)^{2-}$  and  $(\text{UF}_6\text{Cs}_8)^{6+}$  clusters embedded in  $\text{Cs}_2\text{GeF}_6$ , in combination with correlation methods based on multireference wave functions. The local geometry of the impurity-trapped excitons, their potential energy curves, and their multielectronic wave functions have been obtained as direct, nonempirical results of the methods. The calculated excited states appear to be significantly delocalized outside the  $\text{UF}_6$  volume and their U–F bond length turns out to be very short, closer to that of a pentavalent uranium defect than to that of a tetravalent uranium defect. The wave functions of these excited states show a dominant  $\text{U } 5f^17s^1$  configuration character. This result has never been anticipated by simpler models and reveals the unprecedented ability of diffuse orbitals of *f*-element impurities to act as electron traps in ionic crystals. © 2007 American Institute of Physics. [DOI: 10.1063/1.2736703]

## I. INTRODUCTION

A way to transform an insulator into an optically active and often useful luminescent device is to dope it with *f*-element ions. The luminescent properties of the activated solid are related to the  $f^N \rightarrow f^N$  and  $f^{N-1}d^1 \rightarrow f^N$  electronic transitions of the impurity (the so-called localized transitions<sup>1</sup>), but not only. Also important is a less common type of transitions, which was first described by McClure and Pédrini<sup>1</sup> as that in which an electron occupying an impurity state moves to lattice states. An excited state of this kind was recognized in  $\text{Yb}^{2+}$ -doped  $\text{SrF}_2$  and was called an “impurity-trapped exciton” by McClure and Pédrini; it was shown to be responsible for the anomalous emission observed in that crystal. Quoting the authors, an impurity-trapped exciton consists of a bound electron-hole pair with the hole localized on the impurity and the electron on the nearby lattice sites.<sup>1</sup> They describe it further, in the  $\text{SrF}_2:\text{Yb}^{2+}$  case, by proposing that the hole is produced on the  $\text{Yb}^{2+}$  impurity site as the excited electron is delocalized outside the  $\text{YbF}_8$  cluster, over the 12 next  $\text{Sr}^{2+}$  neighbors. This charge spill allows the fluorine ligands to come closer to the effective  $\text{Yb}^{3+}$  impurity, which makes the Yb–F bond length closer to an  $(\text{YbF}_8)^{5-}$  defect.<sup>1</sup> Following the work of McClure and Pédrini, impurity-trapped excitons have been

recognized in a number of wide band gap hosts activated by lanthanide ions and have been found to have a significant role in their luminescence properties (cf. Ref. 2 for a recent review of charge exchange processes in rare earth doped insulating materials). In some cases, like that of  $\text{Yb}^{2+}$ -doped  $\text{SrF}_2$ , the impurity-trapped excitons are supposed to lie below  $f^{N-1}d^1$  impurity states and are held responsible for anomalous emissions like those of  $\text{SrF}_2:\text{Yb}^{2+}$ , which are characterized by a very large Stokes shift relative to the localized  $f^N \rightarrow f^{N-1}d^1$  excitation.<sup>2</sup> In some other cases, they are supposed to lie above  $f^{N-1}d^1$  levels playing a significant role in the dynamics of the electron delocalization from the excited  $f^{N-1}d^1$  levels, which leads to ionization and affects their luminescence efficiency.<sup>3,4</sup> What all these cases have in common is the existence of impurity-trapped excitons postulated in order to account for peculiar spectral features of the activated insulators that cannot be ascribed to the  $f^N$  or  $f^{N-1}d^1$  manifolds alone. However, the microscopic description of impurity-trapped excitons has been quite vague, so far, in terms of “bound electron-hole pairs,” with little description of the nature of the electron state. The characterization of the electronic structure of impurity-trapped excitons is, therefore, a fundamental question.

In this work we present a detailed microscopic characterization of impurity-trapped excitons in  $\text{U}^{4+}$ -doped  $\text{Cs}_2\text{GeF}_6$  crystals. Their electronic structure has been calculated using the relativistic *ab initio* model potential (AIMP)

<sup>a)</sup> Author to whom correspondence should be addressed. Electronic mail: zoila.barandiaran@uam.es

embedded cluster method<sup>5,6</sup> in combination with correlation methods based on multireference wave functions.<sup>7–11</sup> These methods give, as direct, nonempirical results, the local geometry of the impurity-trapped excitons, their potential energy surfaces, and their multielectronic wave functions. The two main microscopic characteristics of impurity-trapped excitons, as envisaged by McClure and Pédrini,<sup>1</sup> are shown by the calculated excited states: (i) their electronic density appears to be significantly delocalized outside the  $\text{UF}_6$  volume and (ii) their U–F bond length turns out to be very short, closer to that of pentavalent uranium defects than to that of tetravalent uranium defects. These excited states are grouped in a rich manifold with wave functions that show a dominant U  $5f^1 7s^1$  configuration character. This result has never been anticipated by simpler models and reveals the unprecedented ability of diffuse orbitals of  $f$ -element impurities to act as electron traps in ionic crystals.

## II. THE ELECTRONIC STRUCTURE OF $5f^1 7s^1$ U-TRAPPED EXCITONS

A number of applications on lanthanide and actinide ions in solids have revealed the adequacy of the relativistic AIMP embedded cluster method,<sup>5,6</sup> in combination with correlation methods based on multireference wave functions,<sup>7–11</sup> as an acceptable methodological framework which allows for the calculation of the local structure around an  $f$ -element impurity and its so-called  $f$ - $f$  and  $f$ - $d$  transitions in ionic crystals. Acceptable compromises between feasibility of the calculations and accuracy of the results have allowed to set reasonable “standard” choices for cluster size, molecular basis sets needed for the molecular orbital expansions, and active spaces that define the multiconfigurational set upon which correlated wave functions are built. These methods and standards have been recently applied to the calculation of the structure and  $5f^2$ - $5f^2$  and  $5f^2$ - $5f^1 6d(t_{2g})^1$  transitions of  $\text{Cs}_2\text{GeF}_6$ : $\text{U}^{4+}$ .<sup>12–14</sup> In this context, in Ref. 13, where the goal was to calculate and measure the  $5f^2 \rightarrow 5f^1 6d^1$  absorption spectrum, excited states with main  $5f^1 7s^1$  configuration were obtained that had not been anticipated and had not appeared, at comparable energies, in similar systems like  $\text{Cs}_2\text{NaYCl}_6$ : $\text{U}^{3+}$  and  $\text{Cs}_2\text{ZrCl}_6$ : $\text{U}^{4+}$  (Refs. 15 and 16, respectively). The  $5f^1 7s^1$  levels were found at energies higher than the  $5f^1 6d(t_{2g})^1$  states and lower than the  $5f^1 6d(e_g)^1$  states (these two latter manifolds correspond to the splitting of the  $5f^1 6d^1$  manifold in the octahedral field experienced by the  $6d$  orbitals at the U site). Inspection of their local geometry and wave functions revealed shorter bond lengths and significantly more diffuse wave functions than those of the  $5f^2$  and  $5f^1 6d(t_{2g})^1$  manifolds, which suggested, on the one hand, their impurity-trapped exciton character, and, on the other hand, the need to question the validity of the standard choices of cluster size, molecular basis set, and active space definitions for the calculation of their electronic structure.

In this work we have explored extensions of the standard choices referred to above so as to ensure acceptable convergence on the energies and wave functions of the  $5f^1 7s^1$  states. The results of this investigation are presented and discussed in Sec. II A where it is shown that large energy sta-

bilizations are obtained as the  $5f^1 7s^1$  wave functions are allowed to delocalize. The electronic structure of the  $5f^1 7s^1$  states, calculated using the new standards, is presented in Secs. II B–II D where the impurity-trapped exciton nature of these excited states is discussed. We address basic questions such as why the  $5f^1 7s^1$  states can be identified with the excited states McClure and Pédrini called impurity-trapped excitons, whether they are impurity states or conduction band states, where the excited electron density resides, and when and why diffuse orbitals of  $f$  elements can be expected to act as electron traps.

### A. Delocalization and energy stabilization

We have investigated the effects of enlarging the cluster size from the usual choice (impurity+first neighbors)  $(\text{UF}_6)^{2-}$  to  $(\text{UF}_6\text{Cs}_8)^{6+}$ , which includes the next eight  $\text{Cs}^+$  cations located at the  $(1/4, 1/4, 1/4)$  crystal sites, forming a cube around the  $\text{UF}_6$  octahedron. Whereas in the new cluster the electronic structure of the  $\text{Cs}^+$  cations has been kept frozen and represented by the same AIMP that were used when these centers were part of the embedding in the  $(\text{UF}_6)^{2-}$  embedded cluster calculations, empty Cs  $6s$  orbitals are now provided which become available for the cluster wave function expansions. The role of the new empty Cs  $6s$  orbitals is twofold. On the one hand, the new atomic functions allow the cluster molecular orbitals to delocalize towards the  $\text{Cs}^+$  sites. On the other hand, they allow to enlarge the reference configurational space with new configurations of the type U  $5f^1$  Cs  $6s^1$ , which would correspond to the suggestion of McClure and Pédrini that the excited electron could be delocalized over the impurity’s second neighbors.<sup>1</sup>

For these purposes, we obtained a  $6s$  atomic orbital from a valence electron Hartree-Fock calculation on the  $6s^1$ - $^2S$  state of Cs using the 13s primitive Gaussian basis functions from Ref. 17 fully uncontracted; the  $\text{Cs}^+$  frozen orbitals were represented by the  $\text{Cs}^+$  AIMP used as embedding potential.<sup>13</sup> This  $6s$  atomic orbital, together with the  $5p$  orbitals of  $\text{Cs}^+$  constitute the minimal  $[1s]$  and  $[1s1p]$  basis sets of Table I. The role of the  $5p$  orbital in the basis set is to allow the molecular orbitals to be orthogonal to the Cs  $5p$  frozen orbitals.<sup>6</sup> Single to quintuple splitting of the  $6s$  orbital (bases  $[2s1p]$  to  $[6s1p]$ ) and addition of one  $p$ -type polarization function from Ref. 18 (bases  $[2s2p]$ ,  $[3s2p]$ ) lead to the other bases of Table I.

The effects of the Cs atomic functions on the transition energies to representative electronic states of the  $5f^1 6d(t_{2g})^1$ ,  $5f^1 7s^1$ , and  $5f^1 6d(e_g)^1$  manifolds are presented in Table I. All the results have been obtained with spin-orbit-free, state-average complete active space self-consistent field (SA-CASSCF) (Ref. 7) embedded cluster calculations, keeping the same active space as in Ref. 13, which generates all the configurations resulting from distributing the two open-shell electrons in 13 active molecular orbitals of symmetry  $a_{2u}$ ,  $t_{1u}$ ,  $t_{2u}$ ,  $t_{2g}$ ,  $e_g$ , and  $a_{1g}$ , whose main character turns out to be U  $5f$ ,  $6d$ , and  $7s$ , respectively; these calculations are referred to as CASSCF ( $5f, 6d, 7s$ ).

The results presented in Table I indicate that the effects of the added functions on the transition energies are negli-

TABLE I. Effects of Cs basis functions on the transition energy to representative electronic states of the  $5f^16d(t_{2g})^1$ ,  $5f^17s^1$ , and  $5f^16d(e_g)^1$  manifolds. The embedded cluster calculations have been done at the CASSCF ( $5f, 6d, 7s$ ) level. In all cases the U[ $6s5p6d5f1g$ ] and F[ $3s4p1d$ ] basis sets of Ref. 13 have been used and the U-F distance is 4.000 bohrs (2.117 Å). Cs atoms are located at the (1/4, 1/4, 1/4) crystal structure sites. All numbers in cm<sup>-1</sup>.

Cluster	Cs basis	Absorption from $5f^2-1^3T_{1g}$					
		$5f^16d(t_{2g})^1$		$5f^17s^1$		$5f^16d(e_g)^1$	
		$1^3E_u$	$1^3A_{1u}$	$1^3A_{2u}$	$2^3E_u$	$2^3A_{2u}$	$3^3E_u$
(UF <sub>6</sub> ) <sup>2-</sup>	None	41 334	41 935	42 452	46 882	70 033	86 346
(UF <sub>6</sub> Cs <sub>6</sub> ) <sup>6+</sup>	[1s]	41 318	41 910	42 439	46 862	68 338	86 360
	[1s1p]	41 315	41 909	42 435	46 859	68 378	86 385
	[2s1p]	41 306	41 882	42 435	46 839	66 601	86 475
	[3s1p]	41 303	41 875	42 435	46 833	65 846	86 520
	[4s1p]	41 314	41 888	42 440	46 841	65 346	86 522
	[5s1p]	41 314	41 889	42 440	46 841	64 991	86 526
	[6s1p]	41 315	41 889	42 441	46 841	64 883	86 523
	[2s2p]	41 310	41 877	42 438	46 837	66 598	86 306
	[3s2p]	41 298	41 867	42 427	46 825	65 593	86 323

gible for the states of the  $5f^16d(t_{2g})^1$  and  $5f^16d(e_g)^1$  manifolds and large for the state representative of the  $5f^17s^1$  manifold. Given that the Cs basis functions added enable the molecular orbitals to transfer electronic density towards the Cs sites, these results indicate the relatively delocalized nature of the  $5f^17s^1$  states. Furthermore, they show that the delocalization of the  $5f^17s^1$  wave functions produces a large energy stabilization (by some 5000 cm<sup>-1</sup>). The results of the [6s1p] basis set appear to be reasonably converged and, therefore, this basis set is our choice for the calculation of the electronic structure of the whole  $5f^17s^1$  and  $5f^16d(e_g)^1$  manifolds presented in this paper in the following subsections.

We have checked other two possible extensions of the molecular basis set. We have supplemented the Cs [3s1p] basis set with one extra *s*-type Gaussian function on the U basis set, which leads to a U [7s5p6d4f1g] basis. Given that the smallest exponent of the *s*-type Gaussian functions of the standard U basis set is 0.026 560 343, the values  $\zeta_s=0.01$  and 0.005 should allow the 7s orbital to be more diffuse, if needed. The results showed negligible effects on the test transition energies and, consequently, this addition was not kept later on. The same is true for the effects of extending the standard molecular basis set with five *s*-type Gaussian functions contracted as [1s], located at the (1/2, 0, 0) interstitial sites, which have been arbitrarily taken as the 2s atomic orbital of the ion embedded in Cs<sub>2</sub>GeF<sub>6</sub>. Their effects on the transition energies investigated was negligible.

As commented above, McClure and Pedrini<sup>1</sup> suggested that the Yb-trapped exciton in SrF<sub>2</sub>:Yb<sup>2+</sup> is formed by a hole produced on the Yb<sup>2+</sup> impurity site and an excited electron which is delocalized outside the YbF<sub>8</sub> cluster, over the 12 next Sr<sup>2+</sup> neighbors. The equivalent description for Cs<sub>2</sub>GeF<sub>6</sub>:U<sup>4+</sup> suggests a hole produced on the U<sup>4+</sup> ions and an excited electron which is delocalized outside the UF<sub>6</sub> cluster, over the eight next Cs<sup>+</sup> neighbors. A possible way to include this in the calculations is to enable the incorporation of the empty molecular orbitals of main character Cs 6s to the active space by adding one set of  $a_{1g}$ ,  $t_{2g}$ ,  $a_{2u}$ , and  $t_{1u}$  empty orbitals to the CAS. The new CASSCF calculations could be labeled CASSCF (U  $5f, 6d, 7s$ ; Cs 6s). In this way,

excited states with main configuration U $5f^1$ Cs $6s^1$  can show up in the wave function and energy calculations at the CASSCF level and beyond. We performed this type of calculations using the U [6s5p6d4f1g], F [3s4p1d], and Cs [3s1p] basis sets. The results reveal that, when they appear, their energies are much higher than those of the states of main configuration  $5f^17s^1$  and  $5f^16d(e_g)^1$ .

## B. Charge leak across the UF<sub>6</sub> boundaries

The results presented in Sec. II A describe, in part, the extent of delocalization of the  $5f^17s^1$  states. On the one hand, they show the delocalization of the  $5f^17s^1$  wave functions, since the orbital mixing with Cs basis functions enables some charge leak towards the Cs sites; furthermore, they indicate that the charge leak produces a large energy stabilization. On the other hand, the results also show that the excited electron is not completely transferred to the Cs cations since this type of excited state occurs at much higher energies. Roughly speaking, it can be said that the excited electron is very delocalized, but is closer to the impurity than it has been expected. In Fig. 1 we show, more precisely, the extent of delocalization through the plots of the molecular natural orbital of main character 7s of the  $5f^17s^1-2^3A_{2u}$  state [plots (a) and (b)] calculated close to its equilibrium distance. Plot (a) shows the equatorial plane of the UF<sub>6</sub> octahedron. Plot (b) shows the plane perpendicular to the (110) axis. Plot (c) shows the 7s atomic orbital calculated in the  $5f^17s^1-3^3F$  excited state of the free U<sup>4+</sup> ion; F labels have been plotted at the coordinates where F atoms appear in the equatorial plot (a) to facilitate comparisons. Plots (d)–(f) are equatorial plots of the molecular natural orbitals of main character  $5f(t_{1u})$ ,  $6d(t_{2g})$ , and  $6d(e_g)$  of  $5f^2-1^3T_{1g}$ ,  $5f^16d(t_{2g})^1-1^3T_{1u}$ , and  $5f^16d(e_g)^1-5^3T_{1u}$  states, respectively, calculated close to their equilibrium geometries. These are also auxiliary plots.

The delocalized nature of the 7s molecular orbital can be clearly concluded from Fig. 1 by comparing the plots (a) and (b) with the 7s atomic orbital in (c), and the plot (a) with the molecular orbitals  $5f(t_{1u})$ ,  $6d(t_{2g})$ , and  $6d(e_g)$  plotted in

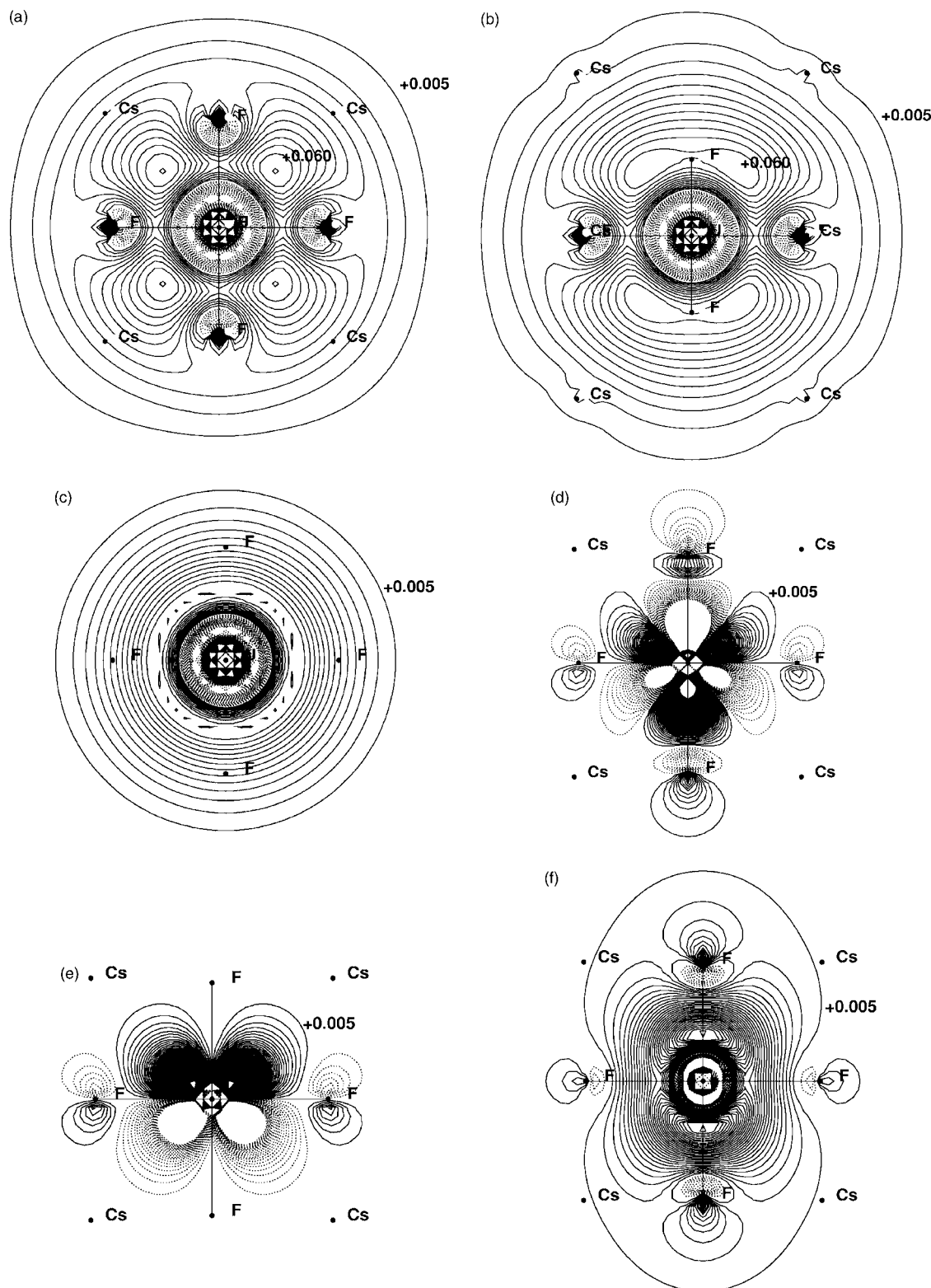


FIG. 1. [(a) and (b)] Molecular natural orbital of main character U  $7s$  in the  $5f^1 7s^1-2\ ^3A_{2u}$  state, calculated at  $R(\text{U}-\text{F})=4.000$  bohrs ( $2.117\ \text{\AA}$ ); cross sections in the equatorial plane of the  $\text{UF}_6$  octahedron and in the plane perpendicular to the  $(110)$  axis. (c)  $7s$  atomic natural orbital of the  $5f^1 7s^1-2\ ^3F$  excited state of the free  $\text{U}^{4+}$  ion; F labels have been plotted at the coordinates where F atoms appear in the equatorial plot (a). [(d), (e), and (f)] molecular natural orbitals of main character U  $5f(t_{1u})$ ,  $6d(t_{2g})$ , and  $6d(e_g)$ , in the  $5f^2-3T_{1g}$ ,  $5f^1 6d(t_{2g})^1-1\ ^3T_{1u}$ , and  $5f^1 6d(e_g)^1-5^3T_{1u}$  states, respectively, calculated at 4.100, 4.100, and 4.200 bohrs ( $2.170$ ,  $2.170$ , and  $2.223\ \text{\AA}$ ), respectively, and plotted in the equatorial plane.

(d)–(e) (all of them in the equatorial plane). The radial extent of the  $7s$  molecular orbital is larger and there is a considerable charge leak across the  $\text{UF}_6$  faces, beyond the maxima observed in the  $(111)$  directions, pointing towards the Cs

sites. The depletion of charge from the  $\text{UF}_6$  interior is quite evident. It is also clear that the charge delocalization occurs in such a way that proximity to the fluorines is avoided.

This picture, together with the energy stabilization ob-



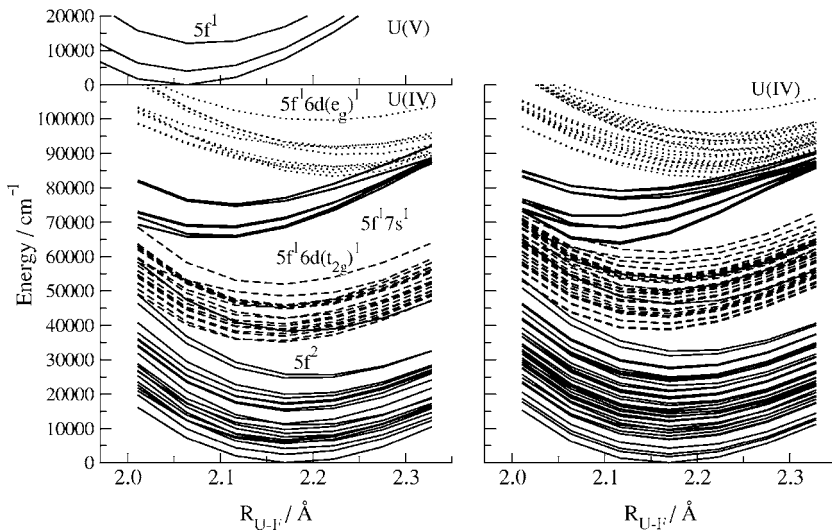


FIG. 2. Breathing mode potential energy curves of  $5f^2$  (solid, thin lines),  $5f^16d(t_{2g})^1$  (dashed lines),  $5f^17s^1$  (solid, thick lines), and  $5f^16d(e_g)^1$  (dotted lines) manifolds of  $\text{Cs}_2\text{GeF}_6:\text{U}^{4+}$ . The  $5f^1$  manifold of  $\text{Cs}_2\text{GeF}_6:\text{U}^{3+}$  is included as an upper part of the left figure. All results include embedding effects and electron correlation. Left: spin-orbit-free calculations. Right: spin-orbit coupling calculations.

served in Sec. II A, suggest the following balance of interactions: When one  $5f$  electron is excited to a very diffuse impurity orbital [like the  $\text{U } 7s$  atomic orbital of Fig. 1(c)] in the small hexafluoride cage, strong electron-electron repulsions occur that can be reduced by a charge spill like that observed in [Figs. 1(a) and 1(b)], withdrawing charge from the cluster interior. In fact, as soon as the wave function is given the flexibility to give charge away, through the use of  $\text{Cs}$  basis functions, it results in large energy stabilizations, as observed in Table I. It should be noted that, in this balance of interactions, the size of the cage formed by the ligands, relative to the extent of the diffuse atomic orbital to which the electron is excited is a key issue. In effect, previous work on  $\text{Cs}_2\text{ZrCl}_6:\text{U}^{4+}$  (Ref. 16) and work in progress in our laboratory indicates that larger ligand cages, such as the  $\text{UCl}_6$  cage, seem to be able to allocate the  $\text{U } 7s$  electron without significant charge spill, that is, allowing the  $7s$  electron charge to stay essentially within the cluster, like regular local states of an  $f$ -element impurity do [Figs. 1(d)–1(f)].

Yet, as mentioned above, the depletion of charge from the  $\text{UF}_6$  volume observed in the  $5f^17s^1$  states of  $\text{Cs}_2\text{GeF}_6:\text{U}^{4+}$  is limited. This is observed in Fig. 1; it is suggested by the convergence of the energy stabilizations of Table I, and it is indicated by the very high energy corresponding to  $\text{U}5f^1\text{Cs}6s^1$  states. This can be taken as an indication that the excited states under study, although delocalized, can still be considered impurity states rather than conduction band states. In this sense the term “impurity-trapped” seems to be appropriate.

### C. Potential energy surfaces: Bond length shrinkage

The calculated potential energy curves of the  $\text{UF}_6$  breathing mode and the spectroscopic parameters (bond lengths,  $R_e$ ; totally symmetric vibrational frequencies,  $\bar{\nu}_{a_{1g}}$ , and minimum-to-minimum energy differences,  $T_e$ ) of the  $5f^2$ ,  $5f^16d(t_{2g})^1$ ,  $5f^17s^1$ , and  $5f^16d(e_g)^1$  manifolds are presented in Fig. 2 and Tables II and III. The results without spin-orbit coupling are presented in Fig. 2 on the left and in Table II; they allow us to deduce the effects of dynamic electron correlation by comparison of CASSCF ( $5f, 6d, 7s$ ) results, which do not include dynamic correlation, with mul-

tistate complete active space second order perturbation calculations,  $\text{MS-CASPT2}(\text{F48}, \text{U20})$ ,<sup>8–11</sup> which include dynamic correlation associated with 68 valence electrons occupying molecular orbitals of main character  $\text{F } 2s, 2p$  and  $\text{U } 5d, 6s, 6p, 5f$ , and  $6d$ . Only the latter have been plotted in Fig. 2. At this same level, the potential energy curves of the  $5f^1$  states of pentavalent uranium defects have been calculated and are shown on the left and upper part in Fig. 2. Results including dynamic correlation and spin-orbit effects (obtained in a second, spin-dependent step, where double-group spin-orbit configuration interaction calculations using the spin-free-state-shifted Wood-Boring AIMP Hamiltonian<sup>6,19,20</sup> are performed), appear in Fig. 2 on the right and in Table III. In all cases, the  $\text{Cs}_2\text{GeF}_6$  host effects have been included in the calculations using the AIMP approximation.<sup>5,6</sup> The results of the  $5f^2$  and  $5f^16d(t_{2g})^1$  manifolds have been obtained in Refs. 12 and 13, respectively; we show here their potential energy curves to favor direct comparisons. Those of the  $5f^17s^1$  and  $5f^16d(e_g)^1$  manifolds have been obtained here and use the extended cluster size and basis set described in Sec. II A. More details of the methods and the calculations are given in Refs. 12 and 13, and references therein.

The potential energy curves plotted on the left of Fig. 2 show that the bond lengths of the  $5f^17s^1$  states (average value:  $2.10 \pm 0.01 \text{ \AA}$ ) are significantly shorter than the bond lengths of the  $5f^2$  manifold (average value:  $2.174 \pm 0.008 \text{ \AA}$  at the same level of calculation) and become significantly closer to the equilibrium distances of the  $5f^1$  states of the pentavalent uranium defect  $\text{Cs}_2\text{GeF}_6:(\text{UF}_6)^{-1}$  (average value:  $2.068 \pm 0.010 \text{ \AA}$ ). Spin-orbit coupling keeps essentially the same picture (Fig. 2, right). This bond length shortening goes together with the depletion of electronic charge from the interior of the  $\text{UF}_6$  volume observed on these states and discussed above, which suggests that the bond shrinkage is a consequence of the electronic charge delocalization across the  $\text{UF}_6$  boundaries. These results support the bond shrinkage assumption of McClure and Pédrini on impurity-trapped excitons as a consequence of the hole created at the impurity site.<sup>1</sup>

Also significant is the increase of the values of the to-

TABLE II. Spectroscopic constants of the  $5f^1 7s^1$  and  $5f^1 6d(e_g)^1$  states of the  $(\text{UF}_6\text{Cs}_8)^{6+}$  cluster embedded in  $\text{Cs}_2\text{GeF}_6$ . Spin-free Hamiltonian calculations. U-F bond distances  $R_e$  (in Å), totally symmetric vibrational frequencies  $\bar{\nu}_{a_{1g}}$  (in  $\text{cm}^{-1}$ ), and minimum-to-minimum energy differences  $T_e$  relative to the  $5f^2-1^3T_{1g}$  ground state (in  $\text{cm}^{-1}$ ). Manifold averages and mean square deviations of the individual values with respect to the averages are labeled as  $\langle 5f^1 7s^1 \rangle$  and  $\langle 5f^1 6d(e_g)^1 \rangle$ .

State	CASSCF ( $5f, 6d, 7s$ )			MS-CASPT2(F48,U20)		
	$R_e$	$\bar{\nu}_{a_{1g}}$	$T_e$	$R_e$	$\bar{\nu}_{a_{1g}}$	$T_e$
$\langle 5f^1 7s^1 \rangle$	$2.11 \pm 0.01$	$575 \pm 29$		$2.10 \pm 0.01$	$605 \pm 43$	
$2^3A_{2u}$	2.104	583	67 842	2.088	595	59 592
$2^1A_{2u}$	2.105	613	68 785	2.086	689	59 957
$3^3T_{2u}$	2.109	538	71 005	2.092	588	62 556
$3^1T_{2u}$	2.109	595	71 064	2.091	602	62 769
$4^3T_{1u}$	2.127	545	76 407	2.109	561	69 166
$4^1T_{1u}$	2.124	577	76 947	2.109	596	69 497
$\langle 5f^1 6d(e_g)^1 \rangle$	$2.24 \pm 0.01$	$576 \pm 83$		$2.22 \pm 0.01$	$493 \pm 69$	
$4^1T_{2u}$	2.240	716	82 320	2.211	586	77 590
$5^3T_{1u}$	2.213	642	82 983	2.231	633	78 624
$3^3E_u$	2.245	511	82 155	2.214	459	79 575
$3^1E_u$	2.240	508	85 318	2.212	455	80 348
$4^3T_{2u}$	2.252	586	83 892	2.229	452	80 444
$5^3T_{2u}$	2.259	631	85 890	2.241	488	83 865
$6^3T_{1u}$	2.254	668	87 730	2.230	522	85 531
$5^1T_{1u}$	2.248	521	91 676	2.217	432	86 091
$5^1T_{2u}$	2.251	505	93 103	2.224	483	86 274
$6^1T_{1u}$	2.251	476	100 316	2.216	418	93 916

tally symmetric vibrational frequencies ( $\bar{\nu}_{a_{1g}}$ ) of the  $5f^1 7s^1$  states compared with the values for the states in the other manifolds (Tables II and III and Refs 12 and 13). This increase is consistent with a higher oxidation state on the uranium impurity on the  $5f^1 7s^1$  states. As a matter of fact, at the MS-CASPT2 level of methodology, the  $\bar{\nu}_{a_{1g}}$  value obtained for the  $5f^1$  states of the pentavalent uranium embedded cluster  $\text{Cs}_2\text{GeF}_6:(\text{UF}_6)^{-1}$  averages  $652 \text{ cm}^{-1}$ , noticeably close to the average value of  $605 \pm 43$  over the  $5f^1 7s^1$  manifold (Table II). These results are an additional indication of charge delocalization away from the impurity site, on the line of McClure and Pédrini impurity-trapped exciton model.<sup>1</sup>

Finally, it is interesting to observe the packing of the  $5f^1 7s^1$  energy levels close to their equilibrium distance, where the interconfigurational interactions do not perturb significantly the shape of the calculated potential energy curves [see  $5f^1 7s^1$  potential energy curves in Fig. 2, close to the energy minima, and the values of minimum-to-minimum energy differences ( $T_e$ ) collected in Tables II and III]. Without spin-orbit coupling, a three-level structure is observed corresponding to  $^3A_{2u}$ ,  $^3T_{2u}$ , and  $^3T_{1u}$  states; the energy difference between the high and low spin states is smaller than  $370 \text{ cm}^{-1}$ . When spin-orbit coupling is included, a five-level grouping is revealed, instead, corresponding to states collected under the labels  $E_{2u}[5/2(^2F)]$ ,  $G_u[5/2(^2F)]$ ,  $E'_{2u}[7/2(^2F)]$ ,  $G'_u[7/2(^2F)]$ , and  $E_{1u}[7/2(^2F)]$ ; the energy differences between sublevels are found to be smaller than  $600 \text{ cm}^{-1}$ . The three-level structure corresponds to the octahedral crystal field splitting of a  $5f$  shell. Analogously, the five-level structure corresponds to the crystal field splitting of the  $5f_{5/2}$ ,  $5f_{7/2}$  spinors. These two energy packings suggest very small  $5f$ - $7s$  electronic interactions, which amount a few

hundreds of wave numbers. They indicate that the  $5f$  and  $7s$  electronic densities are far apart. This is yet another way in which the results of the calculations express the delocalization of the  $7s$  electron.

Altogether, the results presented in this and the previous subsections support the identification of the  $5f^1 7s^1$  states as U-trapped excitons.

#### D. Spectroscopic properties of the $5f^1 7s^1$ U-trapped excitons

The oscillator strengths of the only electric dipole allowed absorptions,  $5f^2-1A_{1g} \rightarrow 5f^1 7s^1-1T_{1u}$ , calculated using the spin-orbit wave functions at the equilibrium distance of the ground state  $2.165 \text{ Å}$  (Table III), are found to be much smaller than the oscillator strength of the most intense  $5f^2-1A_{1g} \rightarrow 5f^1 6d(t_{2g})^1-1T_{1u}$  transition,  $6.55 \times 10^{-2}$  (Ref. 13). This small value (consistent with the atomic selection rule applicable to transitions with  $|\Delta l| > 1$ ) should make it very difficult to detect the  $5f^1 7s^1$  excitons in absorption spectra. They cannot be expected to emit either given the overlap between the  $5f^1 7s^1$  manifold and the higher  $5f^1 6d(t_{2g})^1$  states (see Fig. 2), which should result in very efficient non-radiative decay down to the lowest  $5f^1 6d(t_{2g})^1$  state. However, this efficient nonradiative decay should favour their detection in excitation spectra where emission from the lowest  $5f^1 6d(t_{2g})^1-1E_u$  state is monitored. On the other hand, impurity-trapped excitons lying above the lowest  $f^{N-1}d^1$  states and below the conduction band have been detected through temperature and spectrally resolved photoconductivity studies which allow to deduce the energy difference be-

TABLE III. Results of the calculations on the (UF<sub>6</sub>Cs<sub>8</sub>)<sup>6+</sup> cluster that include Cs<sub>2</sub>GeF<sub>6</sub> embedding, 68 valence electron correlation, and relativistic effects, including spin-orbit coupling. U-F bond distances  $R_e$  (in Å), totally symmetric vibrational frequencies  $\bar{\nu}_{a_{1g}}$  (in cm<sup>-1</sup>), minimum-to-minimum energy differences  $T_e$  relative to the  $5f^2-1A_{1g}$  ground state (in cm<sup>-1</sup>), analyses of the spin-orbit wave functions, and absorption oscillator strengths  $f$ . Manifold averages and mean square deviations of the individual values with respect to the averages are labeled as  $\langle 5f^1 7s^1 \rangle$  and  $\langle 5f^1 6d(e_g)^1 \rangle$ . For comparisons:  $R_e=2.165$  Å for the ground state  $5f^2-1A_{1g}$  (Ref. 12).

State	$R_e$	$\bar{\nu}_{a_{1g}}$	$T_e$	Weights of spin-orbit-free wave functions <sup>a</sup>			$f \times 10^{2b}$
5f <sup>1</sup> 7s <sup>1</sup> manifold <sup>c</sup>							
$\langle 5f^1 7s^1 \rangle$	2.099±0.006	631±70					
$E_{2u}[5/2(^2F)] \times e_{1g}[1/2(^2S)]$							
11 $T_{2u}$	2.097	778	63 516	62.41 2 $^3A_{2u}$	25.98 3 $^3T_{2u}$	11.53 3 $^1T_{2u}$	
4 $A_{2u}$	2.098	743	64 091	58.01 2 $^1A_{2u}$	41.70 3 $^3T_{2u}$		
$G_u[5/2(^2F)] \times e_{1g}[1/2(^2S)]$							
12 $T_{1u}$	2.099	695	68 124	77.42 3 $^3T_{2u}$	14.66 4 $^1T_{1u}$	7.85 4 $^3T_{1u}$	0.000
8 $E_u$	2.096	588	68 368	76.33 3 $^3T_{2u}$	23.58 4 $^3T_{1u}$		
12 $T_{2u}$	2.095	612	68 446	49.79 3 $^1T_{2u}$	25.86 3 $^3T_{2u}$	24.18 4 $^3T_{1u}$	
$E'_{2u}[7/2(^2F)] \times e_{1g}[1/2(^2S)]$							
13 $T_{2u}$	2.090	594	71 480	40.40 3 $^3T_{2u}$	37.44 2 $^3A_{2u}$	22.09 3 $^1T_{2u}$	
5 $A_{2u}$	2.089	633	71 573	58.24 3 $^3T_{2u}$	41.67 2 $^1A_{2u}$		
$G'_u[7/2(^2F)] \times e_{1g}[1/2(^2S)]$							
9 $E_u$	2.104	589	76 837	76.31 4 $^3T_{1u}$	23.57 3 $^3T_{2u}$		
14 $T_{2u}$	2.104	591	76 860	75.65 4 $^3T_{1u}$	16.53 3 $^1T_{2u}$	7.70 3 $^3T_{2u}$	
13 $T_{1u}$	2.103	617	77 027	43.89 4 $^1T_{1u}$	33.66 4 $^3T_{1u}$	22.39 3 $^3T_{2u}$	0.000
$E_{1u}[7/2(^2F)] \times e_{1g}[1/2(^2S)]$							
5 $A_{1u}$	2.104	563	78 823	99.89 4 $^3T_{1u}$			
114 $T_{1u}$	2.106	568	78 891	58.35 4 $^3T_{1u}$	41.38 4 $^1T_{1u}$		0.024
5f <sup>1</sup> 6d(e <sub>g</sub> ) <sup>1</sup> manifold							
$\langle 5f^1 6d(e_g)^1 \rangle$	2.22±0.02	561±72					
15 $T_{2u}$	2.209	619	82 523	47.70 4 $^1T_{2u}$	32.09 5 $^3T_{1u}$		
15 $T_{1u}$	2.208	617	83 879	50.81 4 $^3T_{2u}$	36.34 3 $^3E_u$		2.715
10 $E_u$	2.205	572	84 183	58.09 4 $^3T_{2u}$	32.85 3 $^1E_u$		
16 $T_{2u}$	2.201	622	84 923	40.2 3 $^3E_u$	35.73 4 $^1T_{2u}$	10.38 5 $^1T_{2u}$	
11 $E_u$	2.197	604	85 610	76.98 5 $^3T_{1u}$	13.75 3 $^3T_{2u}$	5.82 4 $^3T_{2u}$	
6 $A_{2u}$	2.232	588	86 206	67.69 5 $^3T_{2u}$	31.26 4 $^3T_{2u}$		
17 $T_{2u}$	2.192	553	86 728	51.76 5 $^3T_{1u}$	26.82 4 $^1T_{2u}$	7.76 5 $^3T_{2u}$	
16 $T_{1u}$	2.192	552	87 019	78.73 5 $^3T_{1u}$	8.46 6 $^3T_{1u}$		0.696
6 $A_{1u}$	2.215	521	87 580	75.62 5 $^3T_{1u}$	18.91 6 $^3T_{1u}$		
17 $T_{1u}$	2.200	560	88 611	29.81 3 $^3E_u$	26.51 4 $^3T_{2u}$	14.01 5 $^1T_{1u}$	1.095
18 $T_{2u}$	2.235	530	89 375	43.25 4 $^3T_{2u}$	41.80 3 $^3E_u$		
12 $E_u$	2.227	516	89 494	57.23 3 $^1E_u$	26.43 4 $^3T_{2u}$		
19 $T_{2u}$	2.245	630	90 405	75.68 5 $^3T_{2u}$	9.64 4 $^1T_{2u}$		
18 $T_{1u}$	2.231	520	90 826	51.25 6 $^3T_{1u}$	14.48 3 $^3E_u$	12.53 4 $^3T_{2u}$	0.336
7 $A_{2u}$	2.242	545	90 955	67.79 4 $^3T_{2u}$	31.11 5 $^3T_{2u}$		
7 $A_{1u}$	2.194	672	91 927	75.74 6 $^3T_{1u}$	22.24 5 $^3T_{1u}$		
13 $E_u$	2.270	748	92 091	80.24 5 $^3T_{2u}$	6.65 4 $^3T_{2u}$	6.48 6 $^3T_{1u}$	
19 $T_{1u}$	2.210	539	93 548	56.54 5 $^3T_{2u}$	17.50 6 $^3T_{1u}$	9.15 5 $^1T_{1u}$	0.153
20 $T_{2u}$	2.230	497	93 557	40.97 6 $^3T_{1u}$	36.80 5 $^1T_{2u}$	15.69 4 $^3T_{2u}$	
14 $E_u$	2.230	527	94 672	87.16 6 $^3T_{1u}$	8.22 5 $^3T_{2u}$		
21 $T_{2u}$	2.245	500	95 391	50.68 6 $^3T_{1u}$	46.84 5 $^1T_{2u}$		
20 $T_{1u}$	2.221	458	95 638	62.56 5 $^1T_{1u}$	27.34 5 $^3T_{2u}$		0.021
21 $T_{1u}$	2.219	410	102 020	91.67 6 $^1T_{1u}$	5.05 6 $^3T_{1u}$		0.003

<sup>a</sup>Only the largest weights are given (in %) and correspond to calculations at  $R(U-F)=2.117$  Å (for the  $5f^1 7s^1$  manifold) and  $R(U-F)=2.223$  Å (for the  $5f^1 6d(e_g)^1$  manifold).

<sup>b</sup>Oscillator strengths for the  $1A_{1g} \rightarrow iT_{1u}$  absorptions were calculated at the ground state equilibrium distance: 2.165 Å.

<sup>c</sup>States within the  $5f^1 7s^1$  manifold are grouped and related to the coupling between (UF<sub>6</sub>)<sup>1-</sup>  $5f^1$  states and one  $s$  electron.

tween the impurity-trapped excitons and the conduction band edge.<sup>3</sup> Analogous research could result in detection of the  $5f^1 7s^1$  excitons in Cs<sub>2</sub>GeF<sub>6</sub>:U<sup>4+</sup>.

The results of the higher  $5f^1 6d(e_g)^1$  manifold are also presented in Fig. 2 and Tables II and III. Their configura-

tional interaction with  $5f^1 7s^1$  states at long U-F distances is quite large, which perturbs the shape of their potential energy curves due to avoided crossings, and affects their equilibrium structure, as it can be seen in Fig. 2 and on the dispersion of the values of  $R_e$  and  $\bar{\nu}_{a_{1g}}$  across the manifold.

### III. CONCLUSIONS

Relativistic *ab initio* model potential calculations on the  $(\text{UF}_6)^{2-}$  and  $(\text{UF}_6\text{Cs}_8)^{6+}$  clusters, which include the quantum mechanical embedding effects of the  $\text{Cs}_2\text{GeF}_6$  host, nondynamical and dynamical correlation of 68 cluster valence electrons, and relativistic effects up to a spin-orbit coupling level, have been done to compute the wave functions and energies of excited states of  $\text{U}^{4+}$  impurities lying above the  $5f^16d(t_{2g})^1$  excited manifold. A set of states of main configuration  $\text{U } 5f^17s^1$  has been found from 63 500 to 79 000  $\text{cm}^{-1}$  that can be identified with the impurity-trapped excitons proposed by McClure and Pédrini<sup>1</sup> in similar materials. Their wave functions are very diffuse, extending beyond the unit made by the  $\text{U}^{4+}$  impurity and its first coordination shell of six fluoride ions, and the U–F bond lengths are very short. The delocalized nature of the excited electron is shown by the results in different ways. A significant orbital mixing between  $\text{U } 7s$  and the second neighbor  $\text{Cs } 6s$  is observed which strongly stabilizes the energy of these states whereas it does not affect the wave functions and energies of the lower  $5f^2$  and  $5f^16d(t_{2g})^1$ , and higher  $5f^16d(e_g)^1$  manifolds. As a result of this charge delocalization, the bond lengths and breathing mode vibrational frequencies become closer to the ones of  $\text{U(V)}$  defects than to  $\text{U(IV)}$  defects, and the energy levels appear to be grouped according to a three-level structure, without spin-orbit, and a five-level structure, with spin-orbit, which corresponds to a  $5f$  electron in an octahedral field, interacting very little with a  $7s$  electron whose electronic density is well separated. The results presented in this paper suggest that as one  $5f$  electron is excited to the very diffuse  $\text{U } 7s$  orbital, which strongly overlaps the electronic density of the small hexafluoride cage, strong electron-electron repulsions occur that provoke a significant charge spill towards the second neighbor  $\text{Cs}$  sites, withdrawing charge from the cluster interior, and allowing for the bond length shrinkage, all of which leads to the formation of impurity-trapped exciton states. Therefore, the size of the repulsive ligand cage, relative to the extent of the diffuse atomic orbital of the impurity, seems to be a driving force for charge spill (small repulsive cage) and formation of an excitonic state or, on the contrary, for the formation of a very high energy local state (large, repulsive cage) whose electron density may still stay within the cluster volume. This explains why in crystals like

$\text{Cs}_2\text{ZrCl}_6:\text{U}^{4+}$  (Ref. 16) and  $\text{Cs}_2\text{NaYCl}_6:\text{U}^{3+}$  (Ref. 15), with larger hexachloride cages,  $5f^17s^1$  excited states appear at higher energies and their electronic structure does not show impurity-trapped exciton characteristics (delocalized density, impurity-ligand bond lengths close to the ionized defect).

### ACKNOWLEDGMENTS

This research was supported in part by Ministerio de Educación y Ciencia, Spain, under Contract No. CTQ2005-08550. One of the authors (B.O.) acknowledges an FPI fellowship from Ministerio de Educación y Ciencia, Spain. The authors dedicate this work to the memory of Professor Lorenzo Pueyo (University of Oviedo), who was Ph.D. supervisor of two of the authors (L.S. and Z.B.).

<sup>1</sup>D. S. McClure and C. Pédrini, Phys. Rev. B **32**, 8465 (1985).

<sup>2</sup>C. Pédrini, Phys. Status Solidi A **202**, 185 (2005).

<sup>3</sup>E. van der Kolk, S. A. Basun, G. F. Imbusch, and W. M. Yen, Appl. Phys. Lett. **83**, 1740 (2003).

<sup>4</sup>E. van der Kolk, P. Dorenbos, J. T. M. de Haas, and C. W. E. van Eijk, Phys. Rev. B **71**, 045121 (2005).

<sup>5</sup>Z. Barandiarán and L. Seijo, J. Chem. Phys. **89**, 5739 (1988).

<sup>6</sup>L. Seijo and Z. Barandiarán, in *Computational Chemistry: Reviews of Current Trends*, edited by J. Leszczyński (World Scientific, Singapore, 1999), Vol. 4, p. 55.

<sup>7</sup>B. O. Roos, P. R. Taylor, and P. E. M. Siegbahn, Chem. Phys. **48**, 157 (1980); P. E. M. Siegbahn, A. Heiberg, J. Almlöf, and B. O. Roos, J. Chem. Phys. **74**, 2384 (1981); P. Siegbahn, A. Heiberg, B. Roos, and B. Levy, Phys. Scr. **21**, 323 (1980).

<sup>8</sup>K. Andersson, P.-Å. Malmqvist, B. O. Roos, A. J. Sadlej, and K. Wolinski, J. Phys. Chem. **94**, 5483 (1990).

<sup>9</sup>K. Andersson, P.-Å. Malmqvist, and B. O. Roos, J. Chem. Phys. **96**, 1218 (1992).

<sup>10</sup>J. Finley, P.-Å. Malmqvist, B. O. Roos, and L. Serrano-Andrés, Chem. Phys. Lett. **288**, 299 (1998).

<sup>11</sup>A. Zaitsevskii and J. P. Malrieu, Chem. Phys. Lett. **223**, 597 (1995).

<sup>12</sup>B. Ordejón, L. Seijo, and Z. Barandiarán, J. Chem. Phys. **123**, 204502 (2005).

<sup>13</sup>B. Ordejón, M. Karbowiak, L. Seijo, and Z. Barandiarán, J. Chem. Phys. **125**, 074511 (2006).

<sup>14</sup>B. Ordejón, V. Vallet, J.-P. Flament, L. Seijo, and Z. Barandiarán, J. Lumin. **126**, 779 (2007).

<sup>15</sup>L. Seijo and Z. Barandiarán, J. Chem. Phys. **118**, 5335 (2003).

<sup>16</sup>Z. Barandiarán and L. Seijo, J. Chem. Phys. **118**, 7439 (2003).

<sup>17</sup>Z. Barandiarán and L. Seijo, Can. J. Chem. **70**, 409 (1992).

<sup>18</sup>J. Andzelm, M. Klobukowski, E. Radzio-Andzelm, Y. Sakai, and H. Tatewaki, in *Gaussian Basis Sets for Molecular Calculations*, edited by S. Huzinaga, (Elsevier, Amsterdam, 1984).

<sup>19</sup>L. Seijo, J. Chem. Phys. **102**, 8078 (1995).

<sup>20</sup>R. Llugar, M. Casarrubios, Z. Barandiarán, and L. Seijo, J. Chem. Phys. **105**, 5321 (1996).